Molecular Systems Biology 4; Article number 211; doi:10.1038/msb.2008.49
**Citation:** ***Molecular Systems Biology*** **4:211**

www.molecularsystemsbiology.com

molecular systems biology

# Variable sizes of *Escherichia coli* chemoreceptor signaling teams

**Robert G Endres[1,2,6], Olga Oleksiuk[3,6], Clinton H Hansen[4], Yigal Meir[5], Victor Sourjik[3,*] and Ned S Wingreen[1,*]**

[1] Department of Molecular Biology, Princeton University, Princeton, NJ, USA, [2] Division of Molecular Biosciences and Centre for Integrated Systems Biology at Imperial College, Imperial College London, London, UK, [3] Zentrum für Molekulare Biologie der Universität Heidelberg (ZMBH), Heidelberg, Germany, [4] Department of Physics, Princeton University, Princeton, NJ, USA and [5] Department of Physics, Ben Gurion University, Beer Sheva, Israel
[6] These authors contributed equally to this work
* Corresponding authors. V Sourjik, Zentrum für Molekulare Biologie der Universität Heidelberg (ZMBH), Im Neuenheimer Feld 282, Heidelberg, Germany. Tel.: +49 622154 6858; Fax: +49 622154 5894; E-mail: v.sourjik@zmbh.uni-heidelberg.de or NS Wingreen, Department of Molecular Biology, Princeton University, Washington Road, Princeton, NJ 08544-1014, USA. Tel.: +1 609 258 1894; Fax: +1 609 258 8616; E-mail: wingreen@princeton.edu

Received 3.4.08; accepted 21.6.08

**Like many sensory receptors, bacterial chemotaxis receptors form clusters. In bacteria, large-scale clusters are subdivided into signaling teams that act as 'antennas' allowing detection of ligands with remarkable sensitivity. The range of sensitivity is greatly extended by adaptation of receptors to changes in concentrations through covalent modification. However, surprisingly little is known about the sizes of receptor signaling teams. Here, we combine measurements of the signaling response, obtained from *in vivo* fluorescence resonance energy transfer, with the statistical method of principal component analysis, to quantify the size of signaling teams within the framework of the previously successful Monod–Wyman–Changeux model. We find that size of signaling teams increases 2- to 3-fold with receptor modification, indicating an additional, previously unrecognized level of adaptation of the chemotaxis network. This variation of signaling-team size shows that receptor cooperativity is dynamic and likely optimized for sensing noisy ligand concentrations.**
*Molecular Systems Biology* 5 August 2008; doi:10.1038/msb.2008.49
*Subject Categories:* simulations and data analysis; signal transduction
*Keywords:* adaptation; chemotaxis; FRET; principal component analysis; receptor clusters



## Introduction

Transmembrane receptors of the chemotaxis network in *Escherichia coli* allow bacteria to sense chemicals in the environment, allowing cells to swim toward nutrients (attractant chemicals) and away from repellents (toxic chemicals). The chemotaxis network possesses remarkable signaling properties, including high sensitivity to small changes in chemical concentration over a wide range of ambient concentrations. These signaling properties rely on receptor clustering (Bray *et al*, 1998), which occurs at multiple length scales. At a small scale, the chemotaxis receptors form stable homodimers, which then assemble into larger complexes in which receptors of different chemical specificities are intermixed (Studdert and Parkinson, 2004; Lai *et al*, 2005). Trimers of dimers (Kim *et al*, 1999; Ames *et al*, 2002; Studdert and Parkinson, 2004) are believed to be the smallest signaling unit (Boldog *et al*, 2006). At a larger scale, ~10 000 receptors form large polar and lateral receptor clusters (Maddock and Shapiro, 1993; Ames *et al*, 2002; Zhang *et al*, 2007). Theoretical analysis of *in vivo* fluorescence resonance energy transfer (FRET) data suggests that large receptor clusters are composed of smaller signaling teams each consisting of about 10 strongly coupled receptor dimers (see Box 1 for details) (Sourjik and Berg, 2004; Mello and Tu, 2005; Keymer *et al*, 2006; Skoge *et al*, 2006), which is consistent with receptor cooperativity (Hill coefficients of dose–response curves) observed *in vitro* (Li and Weis, 2000).

Signal transduction by receptor signaling teams requires association with the kinase CheA, and the adapter protein CheW; both CheA and CheW affect receptor cooperativity (Sourjik and Berg, 2004) and large-scale clustering (Maddock and Shapiro, 1993; Liberman *et al*, 2004; Shiomi *et al*, 2005). CheA's kinase activity is inhibited by attractant binding to receptors. When active, CheA autophosphorylates using ATP and transfers the phosphoryl group to the response regulator CheY. Phosphorylated CheY (CheY-P) diffuses to the flagellar motor and induces clockwise motor rotation and cell tumbling. CheY-P is dephosphorylated by its phosphatase CheZ. In the absence of CheY-P, flagellar motors rotate

**Box 1 Model for receptor signaling**

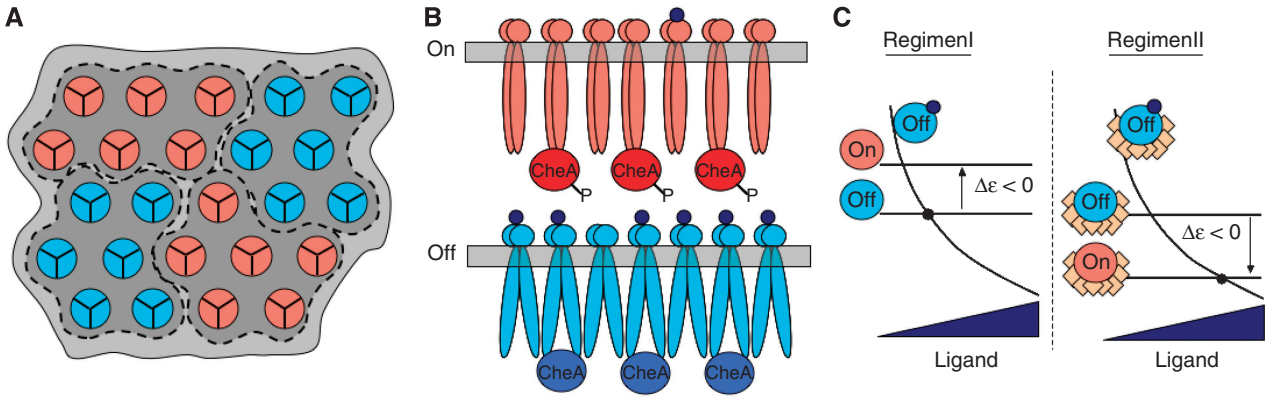


Chemoreceptors cluster at multiple scales ranging from receptor dimers, to trimers of dimers, to large polar and lateral clusters. Signaling properties are believed to arise from groups of several trimers of dimers forming signaling teams. Within a signaling team, receptors are assumed to be coupled strongly enough that the receptors are either all in the on state or all in the off state (**A**). In the on state, the receptor-associated kinase CheA is assumed to be active, autophosphorylating itself and transferring the phospho-group to the response regulators CheY and CheB. In the off state, CheA is inactive and unable to autophosphorylate (**B**). Importantly, the two-state property of the receptor dimers and signaling teams leads to two characteristic regimens of activity as described below.

*Single two-state receptor*: We assume that an individual chemoreceptor (homodimer) has two states, on or off (Asakura and Honda, 1984). Attractant binding favors the off state, in which the receptor-bound kinase CheA is inactive, whereas modification of the receptor favors the on state, in which CheA is active. At equilibrium, the probability that the receptor dimer is on is

$$p_{\mathrm{on}} = \frac{e^{-f^{\mathrm{on}}}}{e^{-f^{\mathrm{on}}}+e^{-f^{\mathrm{off}}}} = \frac{1}{1+e^{\Delta f}}$$

where all energies are expressed in units of the thermal energy $k_{\mathrm{B}}T$. The receptor dimer free-energy difference between on and off states is given by

$$\Delta f = f^{\mathrm{on}} - f^{\mathrm{off}} = \Delta\varepsilon(m) + \log\left(\frac{1+[\mathrm{L}]/K_{\mathrm{D}}^{\mathrm{off}}}{1+[\mathrm{L}]/K_{\mathrm{D}}^{\mathrm{on}}}\right)$$

where ligand binding in the on (off) state with dissociation constant $K_{\mathrm{D}}^{\mathrm{on}}$ ($K_{\mathrm{D}}^{\mathrm{off}}$) is included. For attractant binding $K_{\mathrm{D}}^{\mathrm{off}} < K_{\mathrm{D}}^{\mathrm{on}}$, and for repellent binding, $K_{\mathrm{D}}^{\mathrm{off}} > K_{\mathrm{D}}^{\mathrm{on}}$. The modification state of the receptor dimer enters only through the offset energy $\Delta\varepsilon(m)$. The probability of the on state is considered to be the receptor activity.

Two regimens of activity are apparent. (**C**) A schematic energy-level diagram as a function of attractant (ligand) concentration [L] for a fully demethylated (unmodified) receptor dimer (left, regimen I) and a fully modified receptor dimer (right, regimen II) is shown (Keymer *et al*, 2006). The receptor dimer can either be on or off. For clarity in the figure, only the off state can bind attractant (red disc), with ligand dissociation constant $K_{\mathrm{D}}^{\mathrm{off}}$. Methyl groups or glutamines (diamonds) lower the free energy of the on state. In regimen I, the on-state free energy is above the off-state free energy ($\Delta\varepsilon > 0$) in the absence of attractant, leading to a low activity; the crossing of the lowest levels occurs at $[\mathrm{L}]=K_{\mathrm{D}}^{\mathrm{off}}$ (black dot). In regimen II, the on-state free energy is below the off-state free energy ($\Delta\varepsilon < 0$) in the absence of a ligand, leading to a high activity; the crossing of the lowest levels occurs at an increased ligand concentration $[\mathrm{L}]=K_{\mathrm{D}}^{\mathrm{off}}\exp(|\Delta\varepsilon|)$ (black dot). In both regimens I and II, the crossing of the lowest levels corresponds to the inhibition constant $K_{\mathrm{i}}$ (ligand concentration at half-maximal activity), obtainable from dose–response curves.

*Receptor signaling team*: Within the allosteric Monod–Wyman–Changeux (MWC) model (Monod *et al*, 1965), two-state receptor dimers form signaling teams with all receptors in a team either on or off together (Sourjik and Berg, 2004; Mello and Tu, 2005; Keymer *et al*, 2006). Assuming for simplicity a single receptor type, such as Tar, the equilibrium probability that a signaling team of $N$ receptor dimers will be on is

$$p_{\mathrm{on}} = \frac{e^{-N f^{\mathrm{on}}}}{e^{-N f^{\mathrm{on}}}+e^{-N f^{\mathrm{off}}}} = \frac{1}{1+e^{N\Delta f}}$$

Importantly, signaling-team formation enhances the difference between the two regimens (Keymer *et al*, 2006). In regimen I, where $\Delta\varepsilon > 0$ (e.g. for Tar{EEEE}), receptor dimers have an even lower activity, $\sim\exp(-N\Delta\varepsilon)$, and an inhibition constant $K_{\mathrm{i}} \sim K_{\mathrm{D}}^{\mathrm{off}}/N$, indicating an $N$ times higher sensitivity than that of a single receptor dimer. In regimen II, where $\Delta\varepsilon < 0$ (e.g. for Tar{QQQQ}), receptor dimers are even more fully active, and turn off at attractant concentration $K_{\mathrm{i}} \sim K_{\mathrm{D}}^{\mathrm{off}}\exp(|\Delta\varepsilon|)$ with enhanced cooperativity, specifically with a Hill coefficient $n_{\mathrm{H}} \sim N$.

The strong effect of signaling-team size on the sensitivity of demethylated (unmodified) receptors and on the Hill coefficient of more highly modified receptors allows us to deduce signaling-team size from signaling dose–response curves (Supplementary Table I; Keymer *et al*, 2006; Endres *et al*, 2007).

counterclockwise and the cell runs straight. Adaptation in wild-type cells relies on methylation/demethylation of glutamates at 4–6 specific modification sites (depending on the receptor type) by the enzymes CheR/CheB, the latter being activated through phosphorylation by CheA.

Despite the excellent characterization of much of the bacterial chemotaxis network, very little is known about the sizes of receptor signaling teams, which are difficult to resolve by fluorescence or electron microscopy. However, receptor methylation has been observed to affect polar clustering slightly. Receptor clusters are relatively stable, as demonstrated for polar clusters using fluorescence recovery after photobleaching (Schulmeister *et al*, 2008) and for trimers of dimers (Studdert and Parkinson, 2005) using crosslinking

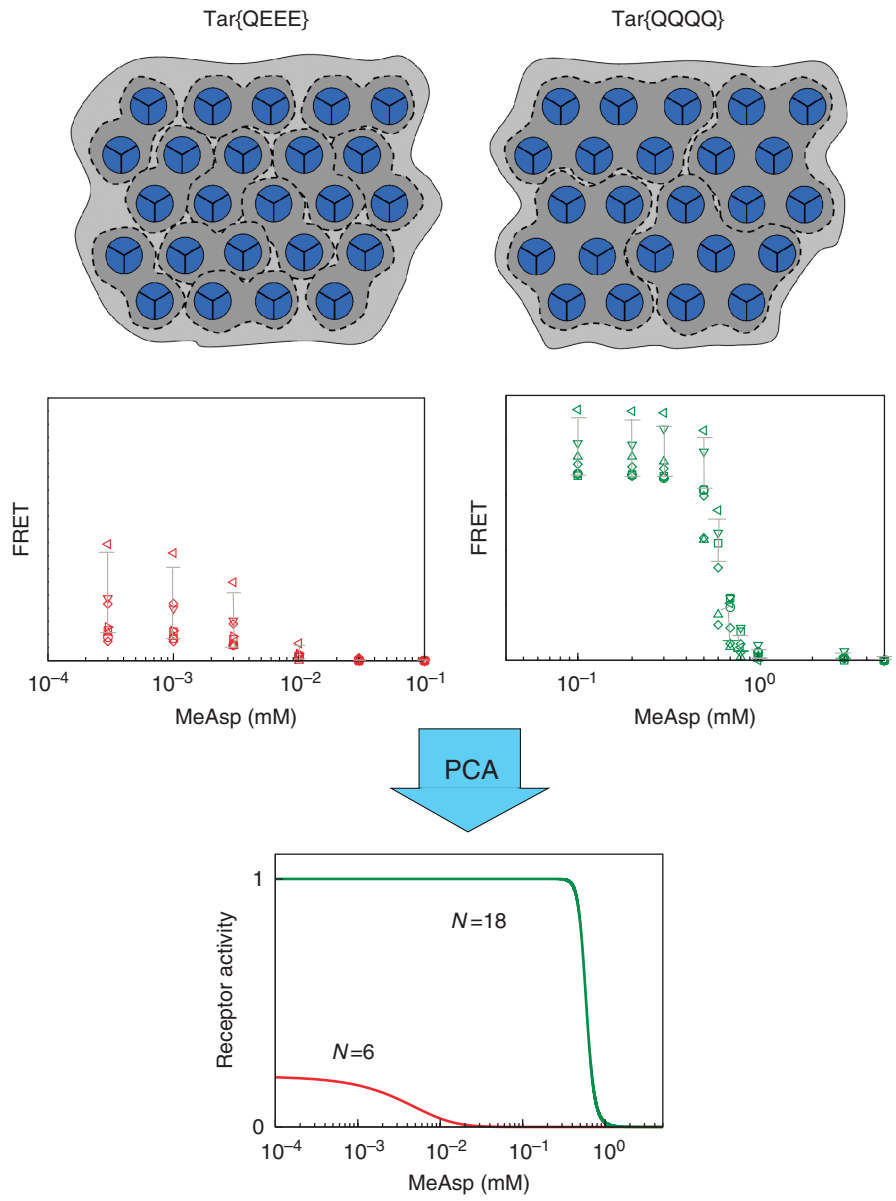


**Figure 1** Determining sizes of receptor signaling teams from signaling dose–response curves. Signaling-team size *N*, i.e. the number of receptor dimers per signaling team, may differ depending on the receptor modification state (glutamate (E) or glutamine (Q) at four specific receptor modification sites). Variable signaling-team sizes are illustrated schematically by membrane patches of trimers of dimers (blue circles) with signaling teams of two trimers (*N*=6 dimers) for Tar{QEEE}, or signaling teams of six trimers (*N*=18 dimers) for Tar{QQQQ}. When directly fitting the free-energy model of receptor activity to the noisy data, the fitted curves and model parameters vary widely, due to the large error bars (middle panel), preventing quantitative analysis of signaling-team sizes. However, use of principal component analysis (PCA) separates the reproducible variation of the data from the sampling noise, allowing quantitative evaluation of parameters, and revealing a systematic dependence of signaling-team size on receptor modification level in living cells.

experiments. However, there is some evidence that demethylation or attractant binding decreases the stability of polar receptor clusters (Shrout *et al*, 2003; Homma *et al*, 2004; Lamanna *et al*, 2005; Vaknin and Berg, 2006), although the effects on the size of the polar and lateral clusters appear to be minor or none (Lybarger and Maddock, 1999; Liberman *et al*, 2004; Lybarger *et al*, 2005; Shiomi *et al*, 2005). *In vitro*, receptor cooperativity has been observed to increase with receptor modification (Li and Weis, 2000), but such an increase in cooperativity is expected with increasing activity even for fixed-size signaling teams (see Box 1; Keymer *et al*, 2006).

Here, we report a method to reliably extract the size of receptor signaling teams from variable *in vivo* FRET signaling data (Figure 1), and apply the method to cells that express only the aspartate-specific Tar receptor. We examined both adapting receptors in the presence of the modification enzymes CheR and CheB, as well as genetically engineered receptors in particular modification states in non-adapting *cheRcheB* cells. To analyze dose–response curves (activity versus MeAsp concentration), we first applied the statistical method of principal component analysis (PCA) to properly treat correlated variability in the data. Next, we fitted our previously established two-state model of signaling to the PCA-treated

data to extract parameters with error bars, including signaling-team sizes and modification-dependent receptor energies. As a result of this quantitative data analysis, we discovered a new level of adaptation in the *E. coli* chemotaxis network. Specifically, we found that signaling-team size increases about three-fold with receptor modification, such as that occurs during adaptation to an attractant. Furthermore, we present a theory that the observed variation in signaling-team size is a novel adaptive mechanism to optimally measure noisy ligand concentrations.

## Results

To measure signal processing by the receptor signaling teams in living bacterial cells under defined conditions, we expressed the high-abundance aspartate chemoreceptor Tar in an otherwise receptorless strain of *E. coli* and used *in vivo* FRET to measure the concentration of CheY-P/CheZ pairs, which is proportional to total CheA activity (Sourjik and Berg, 2002, 2004; Sourjik *et al*, 2007; see Supplementary information). For this purpose, CheY and CheZ were expressed as fusions to yellow (YFP) and cyan (CFP) fluorescent proteins, respectively, which allows energy transfer upon pair formation. From the high sensitivity and cooperativity (Hill coefficient) of dose–response curves previously measured by FRET (Sourjik and Berg, 2002, 2004), and quantitatively interpreted within the Monod–Wyman–Changeux (MWC) model (see Box 1; Monod *et al*, 1965; Sourjik and Berg, 2004; Mello and Tu, 2005; Keymer *et al*, 2006), receptor signaling teams are believed to consist of approximately $N$=10–20 receptor dimers (3–7 trimers of dimers). In the MWC model, a receptor signaling team is an effective two-state system, where all receptors are either on (active) or off (inactive) (Asakura and Honda, 1984), and bind ligand with the dissociation constants $K_D^{on}$ and $K_D^{off}$, respectively. Attractant binding is more favorable in the off state, and hence a high concentration of attractant [L] tends to turn receptors off, whereas receptor modification favors the on state. The probability that a receptor signaling team is active depends only on the free-energy difference between its on and off states, which is $N$ times the free-energy difference of a single receptor, $\Delta F = N\Delta f(\Delta\varepsilon, K_D^{on}, K_D^{off}, [L])$, where $\Delta\varepsilon$ is the free-energy difference in the absence of ligand. $\Delta\varepsilon$ does depend on receptor modification: for unmodified receptors, $\Delta\varepsilon > 0$, whereas for modified receptors, $\Delta\varepsilon < 0$. Only in their on state do receptors induce the kinase activity of receptor-bound CheA. This model has been very successful in describing high sensitivity to ligand, precise adaptation, and signal integration by mixed receptor types (Endres and Wingreen, 2006; Keymer *et al*, 2006), and is believed to reflect an organization of receptors in small tightly coupled signaling teams that are then interlinked to form the large polar and lateral clusters.

Previous studies indicated that increasing receptor modification can enhance protein interactions in receptor clusters (Shrout *et al*, 2003; Shiomi *et al*, 2005; McAndrew *et al*, 2006). To test whether the size of receptor signaling teams depends on the modification state (*cf.* top of Figure 1, showing a schematic of different sized signaling teams of trimers of dimers), Tar receptors were genetically engineered to have either a glutamate (E) or a glutamine (Q) at the four modification sites in the cytoplasmic domain, and expressed in cells lacking all other receptors (see Supplementary information). In chemotaxis, a glutamine (Q) is functionally similar to a methylated glutamate. For instance, strains expressing only Tar{QQQQ} are highly active at zero attractant concentration, whereas strains expressing only Tar{EEEE} are generally inactive. Using α-methyl-DL-aspartate (MeAsp), a non-metabolizable analog of aspartate, we measured dose–response curves, i.e. the activity at various attractant concentrations, for adapting cells (CheRB$^+$) and for non-adapting mutants (*cheRcheB*) that express Tar receptors in different modification states QEEE, QEQE, QEQQ, and QQQQ. The resulting data for each strain show large day-to-day variation (illustrated by the different symbols in Figure 1, middle), despite the fact that the FRET data are intrinsically independent of the number of measured cells, as only fluorescence ratios are considered. The variation presumably stems from a fluctuating expression of the Tar receptor even at a defined inducer concentration. Because of the large error bars on the data, a standard $\chi^2$ analysis provides only a weak constraint on signaling-team size. However, the variation of the data is highly correlated, e.g. the overall amplitudes of dose–response curves vary considerably, whereas the shapes remain more consistent. To exploit this consistency of the data, we used the statistical method of PCA (Figure 2, see Materials and methods, and Supplementary information). Given a set of dose–response curves, PCA identifies the independently varying collective modes of the data, specifically a highly variable amplitude mode and multiple, less variable shape modes. Within standard $\chi^2$ analysis, deviations between model and data are weighted by the inverse of the variance at each data point. In contrast, our fits of the MWC model to the data are weighted by the inverse variance of the PCA modes, exploiting our greater confidence in the least variable modes of the data. A sufficient number of principal components are included to account for most of the data variation while not overinterpreting the data due to small sample size (Supplementary Figure 6). As a result, we were able to obtain tight error bars on model parameters and to draw quantitative conclusions on the variation of signaling-team size with receptor modification. As a schematic example, Figure 1 (bottom) shows illustrative high-confidence fits, indicating that the number of receptor dimers per Tar{QEEE} and Tar{QQQQ} signaling team is $N \sim 6$ and $\sim 18$ receptor dimers, respectively.

Figure 3 shows experimental dose–response curves (symbols) for all strains at high (about 3.6 × native) Tar expression level, as well as the corresponding theoretical best fits obtained using PCA (curves) (see Supplementary Figure 7 for the data and fits at low (about 1.4 × native) Tar expression level). The results for both expression levels are summarized in Figure 4, which shows the inferred signaling-team sizes $N$ (top) and receptor offset energies $\Delta\varepsilon$ (bottom) for low (left) and high (right) Tar receptor expression levels: An increase in signaling-team size with increasing receptor modification is apparent, ranging from 5 to 7 receptor dimers for Tar{QEEE} to 16–19 receptor dimers for Tar{QQQQ} (depending on receptor expression). On the basis of our error bars, at low expression level, signaling-team sizes for Tar{QEEE} and Tar{QEQE} are conclusively smaller than for Tar{QQQQ}, i.e. $N_{QEEE}$, $N_{QEQE} < N_{QQQQ}$, and at high expression level

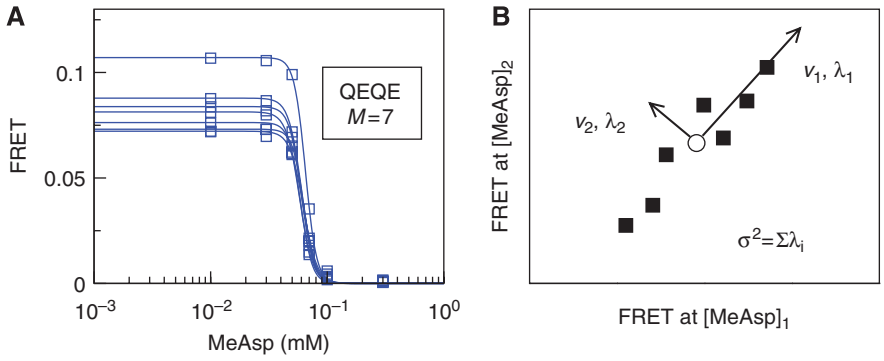


**Figure 2** Illustration of principal component analysis (PCA) applied to dose–response curves of receptor activity to obtain principal modes of data variation. Receptor activity at various concentrations of attractant (MeAsp) was measured through *in vivo* FRET for *E. coli* cells expressing only Tar receptors. (**A**) Measured dose–response curves show large variability, as exemplified by $M=7$ individual curves for the receptor modification state QEQE in a *cheRcheB* mutant. (**B**) Illustration of a scatter plot of data from (A) in a space of dimension $D$ equal to the number of different attractant concentrations (projected onto two dimensions for clarity). Each data point (square) corresponds to one dose–response curve. The average dose–response curve is shown as an open circle. PCA involves diagonalizing the covariance matrix $C$, where the principal components—eigenvectors $\boldsymbol{\nu}_i$ and eigenvalues $\lambda_i$ of $C$ with $i=1,\ldots, D$—indicate the direction and magnitude of variation of the data. The sum of the eigenvalues equals the total variance of the data. The open square illustrates our practice of leaving out one data point when determining the optimal number of principal components to be included for fitting (see Supplementary Figure 6B).

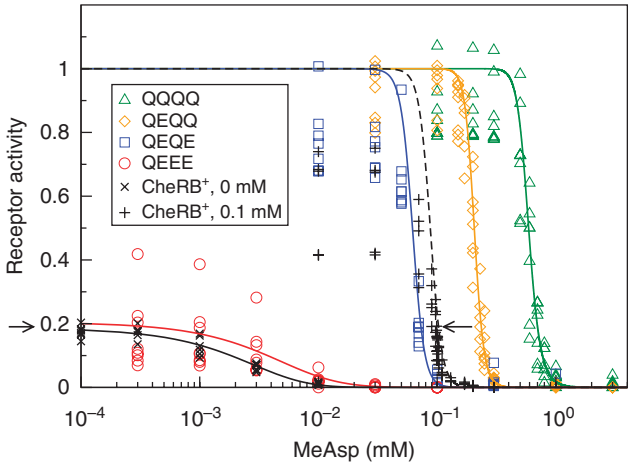


**Figure 3** Individual receptor-activity dose–response curves (symbols) and corresponding PCA fits (solid lines) for *E. coli* cells expressing only Tar receptors at high ($\sim 3.6\times$ native) expression level (see Supplementary information). Cell types include adapting ($CheRB^+$) and non-adapting, engineered *cheRcheB* mutants (QEEE, QEQE, QEQQ, and QQQQ). $CheRB^+$ cells are adapted either to zero attractant (x symbols) or to 0.1 mM MeAsp ($+$ symbols). The arrows indicate the adapted activity of 0.2. Measurement of the dose–response curves of $CheRB^+$ cells adapted to 0.1 mM MeAsp required not only addition but also removal of MeAsp. The experimental data were normalized by the inverse amplitude $\phi^{-1}$ (see Materials and methods, and Supplementary Table I).

$N_{QEEE} < N_{QEQE} < N_{QEQQ}$, $N_{QQQQ}$ (see Supplementary Table I for numerical values of parameters). Additionally, receptor offset energies $\Delta\varepsilon$ decrease systematically with modification state and are approximately independent of receptor expression level, as expected for an intrinsic single-receptor property, providing further evidence for the reliability of our data acquisition and analysis.

Our results indicate that the size of receptor signaling teams depends directly on receptor modification state, not on receptor activity. The Tar{QEQE}, Tar{QEQQ}, and Tar{QQQQ} strains are all fully active at low MeAsp concentrations (see Figure 3 and Supplementary Figure 7), but signaling-team size nevertheless increases with the number of glutamines (Figure 4). To further test the dependence of signaling-team size on receptor modification at high Tar expression level, we made use of the fact that $CheRB^+$ cells adapted to two different attractant concentrations, 0 and 0.1 mM MeAsp, have the same activity (indicated by arrows in Figure 3), but, respectively, low and high receptor modification levels. Compared to cells adapted to zero ambient, the receptor methylation level (as evident from the offset energy) and signaling-team size have significantly increased for cells adapted to 0.1 mM MeAsp (plus symbols in Figure 3 and stripe pattern in Figure 4B and D).

To test whether our results for the sizes of receptor signaling teams depended on the MWC model, we also obtained fits of the FRET data using alternative models in which trimers of dimers are coupled to their nearest neighbors in a triangular or in a honeycomb lattice (see Supplementary information). Although these Ising-type lattice models do not account well for the data from mostly demethylated receptors (Skoge *et al*, 2006), adequate fits to dose–response curves were obtained for the more highly modified receptors. The results strongly confirm our conclusion that effective signaling-team size increases significantly with receptor modification.

Do the observed variable complex sizes reflect an 'optimal' receptor signaling-team size that changes with ligand concentration? We address this question briefly here, with details in the Supplementary information. Complexes of $N$ receptor dimers respond more strongly to changes in ligand concentration than do single receptor dimers, as the free-energy difference of a receptor signaling team is $N\Delta f$, where $\Delta f$ is the free-energy difference of a single receptor dimer. Hence larger signaling teams are better for detecting weak signals. However, larger signaling teams are also noisier than smaller signaling teams, as ligand noise gets amplified as well. For instance, the standard deviation of the free-energy difference of a signaling team due to ligand concentration noise $\delta[L]$ is

$$\sigma_F = N\frac{d(\Delta f)}{d[L]}\delta[L] \qquad (1)$$

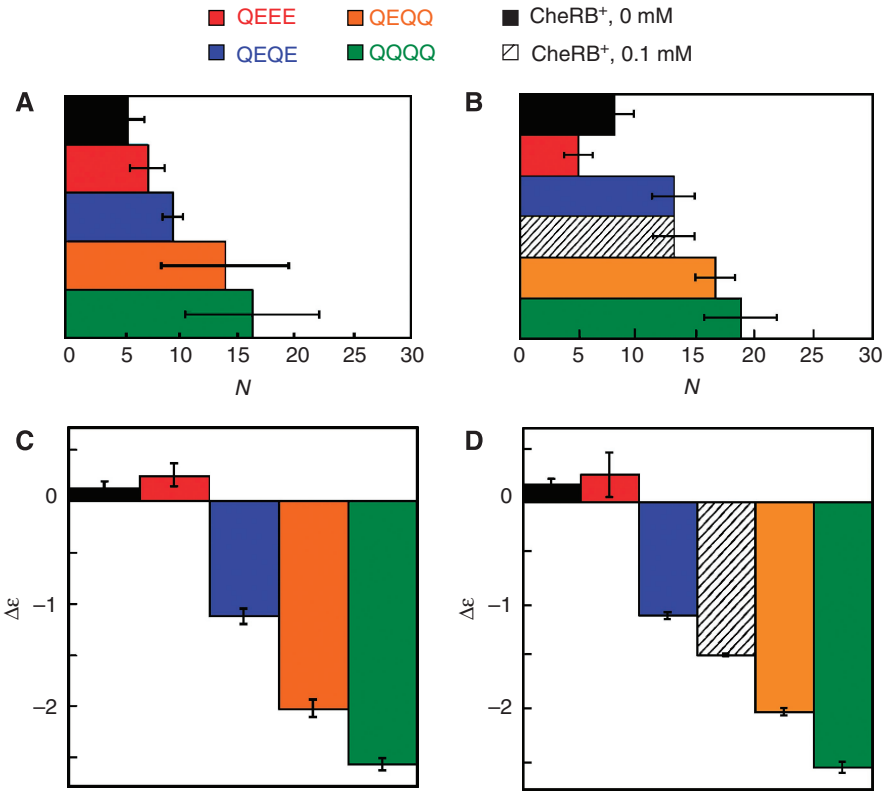


**Figure 4** Sizes of receptor signaling teams *N* (number of receptor dimers per signaling team, panels **A** and **B**) and offset energies $\Delta\varepsilon$ (panels **C** and **D**) obtained from PCA fits shown in Figure 3 in the main text and Supplementary Figure 7. The left panels A and C correspond to low ($\sim 1.4\times$ native) expression of Tar receptors, whereas the right panels B and D correspond to high ($\sim 3.6\times$ native) expression (see Materials and methods). Cell types include adapting (CheRB$^+$) and non-adapting, engineered *cheRcheB* mutants (QEEE, QEQE, QEQQ, and QQQQ). For numerical values of parameters and confidence intervals, see Supplementary Table I.

where the derivative is

$$\frac{\mathrm{d}(\Delta f)}{\mathrm{d}[\mathrm{L}]} = \frac{1}{K_\mathrm{D}^\mathrm{off} + [\mathrm{L}]} - \frac{1}{K_\mathrm{D}^\mathrm{on} + [\mathrm{L}]} \qquad (2)$$

A large standard deviation of the free-energy difference of a signaling team, i.e. $\sigma_\mathrm{F} > 1$ in units of the thermal energy $k_\mathrm{B}T$, means that many signaling teams are either fully active or fully inactive, making them unresponsive to small changes in the mean ligand concentration, and therefore of no use for chemotaxis. A restriction to $\sigma_\mathrm{F} \lesssim 1$ sets an upper limit on the size of signaling teams. The lowest possible uncertainty in ligand concentration is given by the Berg and Purcell limit (Berg and Purcell, 1977) and generalized by Bialek and Setayeshgar (2005) $\delta[\mathrm{L}]/[\mathrm{L}] = 1/\sqrt{\pi a D [\mathrm{L}] \tau}$, where $a$ is the receptor dimension, $D$ is the ligand diffusion constant, and $\tau$ is the averaging time. On the basis of this estimate, equation (1) can be solved for the upper limit on the signaling-team size

$$N \lesssim \frac{\sqrt{\pi a D [\mathrm{L}] \tau}}{[\mathrm{L}]/([\mathrm{L}] + K_\mathrm{D}^\mathrm{off}) - [\mathrm{L}]/([\mathrm{L}] + K_\mathrm{D}^\mathrm{on})} \qquad (3)$$

As a result, to optimize sensitivity the signaling-team size increases as $N \sim [\mathrm{L}]^{1/2}$ for intermediate ligand concentrations ($K_\mathrm{D}^\mathrm{off} \ll [\mathrm{L}] \ll K_\mathrm{D}^\mathrm{on}$). In a nutshell, larger signaling teams are more sensitive to small changes in ligand concentration, but as a result are also more sensitive to ligand concentration noise. Optimally, signaling teams will be as large as possible without being saturated by this noise (i.e. fully active or fully inactive and hence unresponsive to ligand concentration changes). As the relative ligand noise decreases with concentration, the optimal signaling-team size will grow with ligand concentration, as we observed.

## Discussion

The chemotaxis network of *E. coli* exhibits remarkable sensing and signaling properties that rely on receptor signaling teams. Despite recent high-resolution electron microscopy (Weis *et al*, 2003; McAndrew *et al*, 2004, 2005, 2006; Briegel *et al*, 2008), very little is known about what determines receptor signaling-team formation and size (Kentner and Sourjik, 2006; Kentner *et al*, 2006). Notably, because signaling-team size and signaling sensitivity are closely related (Keymer *et al*, 2006; Endres *et al*, 2007; Mello and Tu, 2007), receptor kinase activity can be used to probe signaling-team size. Starting from dose–response data on the activity of Tar receptors from *in vivo* FRET experiments, we developed a robust analysis method to extract signaling-team sizes and receptor offset energies (Figure 1), interpreted within a well-established model for cooperative receptor signaling (see Box 1). To achieve this, we applied the unbiased statistical method of PCA (see Figure 2, Materials and methods, and Supplementary information) to the data to separate correlated variation in the data from noise due to small sample size. Conventional $\chi^2$ fitting to individu-

ally normalized data curves misses the comparison of amplitudes, and when applied to averaged data values and their standard deviations overestimates the fluctuations by missing the correlations among the data points within a dose–response curve measured on the same day. Using our PCA analysis, we then fitted the MWC model for receptor signaling teams (see Box 1) to the principal components of the data, allowing us to obtain receptor parameters with tight confidence intervals (Figures 3 and 4, as well as Supplementary Figure 7). Importantly for chemotaxis, we found that signaling-team size increases significantly with receptor modification level (Figure 4). Motivated by this discovery, we presented a model describing how variable signaling-team size may enable cells to optimally measure ligand concentrations. Whereas both small changes in ligand concentration (signal) and ligand concentration noise are increasingly amplified by increasing signaling-team size, the noise decreases for increasing ambient concentration. This allows the cell to utilize larger signaling teams at larger ambient concentrations and hence receptor modification levels without saturation of the signaling teams by noise.

Our results based on Tar-only mutants suggest a previously unrecognized level of adaptation relying on increasing signaling-team size with receptor modification. Interestingly, the opposite trend, i.e. a diminishing ability to cluster with increasing receptor modification, was suggested to possibly downregulate overall sensitivity with adaptation (Bray *et al*, 1998). In the MWC model, however, this downregulation simply emerges from the two-state property (Box 1 and Keymer *et al*, 2006). To show that variable signaling-team sizes also apply to mixed receptor types, a similar detailed analysis would need to be conducted on FRET data of wild-type cells. As Tsr and Tar are the most abundant receptor types, at least the numbers of Tsr and Tar receptor dimers per receptor signaling team would need to be considered while ensuring that the overall ratio of Tsr/Tar stays independent of modification state. Previous standard analysis of such FRET data showed that mixed Tar/Tsr signaling teams contain a total of around 10–20 receptor dimers, consistent with our Tar signaling teams. Additionally, as wild-type cells show high degree of polar clustering (Maddock and Shapiro, 1993; Sourjik and Berg, 2000; Liberman *et al*, 2004), the deduced clustering ability of Tar receptors is not an artifact of the homogeneous receptor expression.

What are the possible mechanisms responsible for receptor signaling-team formation and the increase in signaling-team size with increasing receptor modification? Receptor modification reduces the electrostatic repulsion between neighboring dimers by removing charged glutamate residues, potentially stabilizing larger signaling teams. However, the modification sites of neighboring receptor dimers are at least 3 nm apart in the partial crystal structure (Kim *et al*, 1999). For a Debye–Hückel screening length of 1 nm, the resulting screened electrostatic interaction is only 1% of the thermal energy for a pair of charged glutamates. Therefore, other mechanisms may contribute to the observed dependence of signaling-team size on receptor modification: (1) binding of CheA and CheW affects both large-scale clustering of receptors (Maddock and Shapiro, 1993; Sourjik and Berg, 2000; Liberman *et al*, 2004) and the sizes of signaling teams (Sourjik and Berg, 2004), and the relevant binding affinities of CheA and CheW appear to depend on the level of receptor modification (Shrout *et al*, 2003); (2) receptor activity has been shown to respond to receptor–membrane interactions (Draheim *et al*, 2006) and changes in osmotic pressure (Vaknin and Berg, 2006), so inter-dimer coupling could be mediated by elastic membrane deformations, as proposed for the approximate two-state osmolarity-sensing MscL pore (Ursell *et al*, 2007). Our data also indicate that signaling-team size increases moderately with expression level (Figure 4 and Supplementary Table I), perhaps because more available receptors push the distribution of signaling teams toward larger sizes (Endres *et al*, 2007).

Many other sensory systems cluster, including B cell (Schamel and Reth, 2000), T cell (Germain and Stefanova, 1999), synaptic (Griffith, 2004), and ryanodine (Yin *et al*, 2005), indicating that receptor clustering is an important regulatory mechanism for the cell, e.g. to adjust signaling properties or by recruiting auxiliary proteins. As eukaryotic G-protein-coupled receptors become covalently modified as well, e.g. by phosphorylation, receptor modification may prove to be a general mechanism for dynamic regulation of cluster size and optimization of signal response.

## Materials and methods

### Model for receptor signaling team

To extract parameters of receptor signaling teams from fitting to *in vivo* FRET data, we describe signaling teams by the allosteric MWC model (Monod *et al*, 1965), as described in Box 1. Briefly, in this model signaling teams are composed of two-state receptors with all receptors in a signaling team either on or off together (Sourjik and Berg, 2004; Keymer *et al*, 2006). The number of receptor dimers per signaling team is treated as a continuous parameter, reflecting the degree of cooperativity among receptors, independent of the suborganization of dimers into trimers of dimers. Assuming a single receptor type, such as Tar, the equilibrium probability that an MWC signaling team of $N$ receptor dimers will be on is

$$p_{\mathrm{on}} = \left(1 + \exp\left[N\left\{\Delta\varepsilon(m) + \log\left(\frac{1+[\mathrm{L}]/K_{\mathrm{D}}^{\mathrm{off}}}{1+[\mathrm{L}]/K_{\mathrm{D}}^{\mathrm{on}}}\right)\right\}\right]\right)^{-1} \qquad (4)$$

where $\Delta\varepsilon(m)$ is the offset energy, which depends on the receptor modification level $m$, [L] is the attractant concentration, and $K_{\mathrm{D}}^{\mathrm{on(off)}}$ is the attractant dissociation constant in the on (off) state. All energies are expressed in units of the thermal energy $k_{\mathrm{B}}T$. We obtain the signaling-team size $N$ and the modification-dependent off-set energies $\Delta\varepsilon(m)$ from the fitting procedure described next. The attractant dissociation constants for the on and off states are taken from Keymer *et al* (2006).

### PCA

To obtain $\chi^2$ fits, including confidence intervals for parameters, it requires a representation of the data where deviations from average values are uncorrelated. This is achieved by diagonalizing the covariance matrix of the data for each strain to obtain the principal (uncorrelated) components of the data (see Supplementary Figure 5). Specifically, from the $M$ dose–response curves $x_{i=1,\ldots,M}(L)$, each measured for $D$ different ligand concentrations $L$, the $D \times D$ covariance matrix $C$ is calculated through

$$C(L_1, L_2) = \frac{1}{M}\sum_{i=1}^{M}[x_i(L_1) - x_{\mathrm{ave}}(L_1)][x_i(L_2) - x_{\mathrm{ave}}(L_2)] \qquad (5)$$

where $L_1$ and $L_2$ are ligand concentrations, and $x_{\mathrm{ave}}(L)$ is the average of all $M$ curves at concentration $L$. Each covariance matrix is diagonalized by $V^{-1}CV{=}U$ where $V$ is a matrix with the eigenvectors of $C$ as the

columns and $U$ is the diagonal matrix of the eigenvalues $\lambda_{m=1,\ldots,D}$. These eigenvectors and eigenvalues are the principal components of the data. Standard fitting of a calculated curve $c(\nu; L)$, which depends on a set of fitting parameters $\nu$, to $x_{\mathrm{ave}}$ would require minimizing

$$\chi^2 = \sum_{j=1}^{D} \left( \frac{[c(L_j) - x_{\mathrm{ave}}(L_j)]}{\sigma_{L_j}} \right)^2 \quad (6)$$

where $\sigma_L$ is the experimental standard deviation of the data at ligand concentration $L$. But this neglects the observed correlations within each dose–response curve (*cf.* Figure 2A). Instead, we express $\chi^2$ in the PCA basis set by using $\tilde{c}=V^{-1}(c-x_{\mathrm{ave}})$ and replacing the sum over $D$ ligand concentrations by the sum over $D$ principal components

$$\chi^2_{\mathrm{PCA}} = \sum_{m=1}^{D} \frac{\tilde{c}_m^2}{\lambda_m} \quad (7)$$

For fits using equation (7), we included only the 3–5 largest principal components (see Supplementary Figure 6). We fitted the data for all five strains QQQQ, QEQQ, QEQE, QEEE, and CheRB$^+$ simultaneously by minimizing the total $\chi^2_{\mathrm{PCA}}$, as one fitting parameter, an overall amplitude factor $\phi$, is common to all five strains. The calculated dose–response curve for each strain also depends on an offset energy $\Delta\varepsilon$ and signaling-team size $N$, leading to a total of 11 fitting parameters $\nu=(\phi, \Delta\varepsilon_1, N_1, \ldots, \Delta\varepsilon_5, N_5)$ for the low expression level data (*cf.* Supplementary Figure 7A and Figure 4A), and 13 fitting parameters $\nu=(\phi, \Delta\varepsilon_1, N_1, \ldots, \Delta\varepsilon_6, N_6)$ for the high expression level data (*cf.* Figures 3 and 4B). The dissociation constants for MeAsp binding by Tar in the on and off states were taken to be $K_{\mathrm{D}}^{\mathrm{on}}=0.5$ and $K_{\mathrm{D}}^{\mathrm{off}}=0.02$ mM, respectively (Keymer *et al*, 2006).

## Confidence intervals

We followed the method of Press *et al* (2002), but expressed the curvature matrix

$$\alpha = \frac{\partial^2 \chi^2}{\partial \nu_k \partial \nu_l} \sim 2 \sum_{j=1}^{D} \frac{1}{\sigma_{L_j}^2} \frac{\partial c(L_j)}{\partial \nu_k} \frac{\partial c(L_j)}{\partial \nu_l} \quad (8)$$

in the PCA basis by transforming $\tilde{c}=V^{-1}(c-x_{\mathrm{ave}})$ and calculating

$$\alpha_{\mathrm{PCA}} \sim 2 \sum_{m=1}^{D} \frac{1}{\lambda_m} \frac{\partial \tilde{c}_m}{\partial \nu_k} \frac{\partial \tilde{c}_m}{\partial \nu_l} = 2B^{\mathrm{T}}AB \quad (9)$$

with $A=(V^{-1})^{\mathrm{T}}U^{-1}V^{-1}$ and $B_{\mathrm{qk}}=\partial c(L_{\mathrm{q}})/(\partial \nu_{\mathrm{k}})$. Confidence intervals were obtained from the total ($\alpha^{\mathrm{tot}}_{\mathrm{PCA}}$) summed over the five strains. From the corresponding covariance matrix $C^{\alpha}=(\alpha^{\mathrm{tot}}_{\mathrm{PCA}})^{-1}$, the confidence interval of parameter $\nu_{\mathrm{k}}$ is given by $\delta\nu_{\mathrm{k}} = \pm\sqrt{\Delta\chi^2}\sqrt{C^{\alpha}_{\mathrm{kk}}}$ where $\Delta\chi^2=4$ for 95.4% confidence.

## Experimental protocol

Cell growth, FRET measurements, and immunoblots were performed essentially as before (Sourjik and Berg, 2002, 2004; Sourjik *et al*, 2007). Briefly, receptorless cells co-expressing a CheZ-CFP/CheY-YFP FRET pair and Tar receptors in one of the modification states were grown to mid-exponential phase in the presence of appropriate antibiotics. Expression of the FRET pair was induced with 50 μM isopropyl β-D-thiogalactoside. Expression of receptors was induced with either 1 or 2 μM sodium salicylate, corresponding to low and high levels, respectively. Cells were harvested, washed, and assayed for attractant-induced changes in FRET signal in a flow chamber mounted on a custom-modified Zeiss Axiovert 200 microscope. Fluorescence of a field of 300–500 cells was monitored in each experiment. FRET was defined as the fractional change in cyan fluorescence due to energy transfer, and was calculated from changes in the ratios of yellow and cyan fluorescence signals (Sourjik and Berg, 2004). See Supplementary information for measurement details and for the list of strains and plasmids used in this study.

## Supplementary information

Supplementary information is available at the *Molecular Systems Biology* website (www.nature.com/msb).

# Acknowledgements

We thank Fred Hughson, Tom Shimizu, Monica Skoge, and Chris Wiggins for helpful suggestions. All authors (except CHH) acknowledge funding from the Human Frontier Science Program (HFSP).

# References

Ames P, Studdert CA, Reiser RH, Parkinson JS (2002) Collaborative signaling by mixed chemoreceptor teams in *Escherichia coli*. *Proc Natl Acad Sci USA* **99:** 7060–7065

Asakura S, Honda H (1984) Two-state model for bacterial chemoreceptor proteins. The role of multiple methylation. *J Mol Biol* **176:** 349–367

Berg HC, Purcell EM (1977) Physics of chemoreception. *Biophys J* **20:** 193–219

Bialek W, Setayeshgar S (2005) Physical limits to biochemical signaling. *Proc Natl Acad Sci USA* **102:** 10040–10045

Boldog T, Grimme S, Li M, Sligar SG, Hazelbauer GL (2006) Nanodiscs separate chemoreceptor oligomeric states and reveal their signaling properties. *Proc Natl Acad Sci USA* **103:** 11509–11514

Bray D, Levin MD, Morton-Firth CJ (1998) Receptor clustering as a cellular mechanism to control sensitivity. *Nature* **393:** 85–88

Briegel A, Ding HJ, Li Z, Werner J, Gitai Z, Dias DP, Jensen RB, Jensen G (2008) Location and architecture of the *Caulobacter crescentus* chemoreceptor array. *Mol Microbiol* **68:** 30–41

Draheim RR, Bormans AF, Lai RZ, Manson MD (2006) Tuning a bacterial chemoreceptor with protein–membrane interactions. *Biochemistry* **45:** 14655–14664

Endres RG, Falke JJ, Wingreen NS (2007) Chemotaxis receptor complexes: from signaling to assembly. *PLoS Compl Biol* **3:** e150

Endres RG, Wingreen NS (2006) Precise adaptation in bacterial chemotaxis through 'assistance neighborhoods'. *Proc Natl Acad Sci USA* **103:** 13040–13044

Germain RN, Stefanova I (1999) The dynamics of T cell receptor signaling: complex orchestration and the key roles of tempo and cooperation. *Annu Rev Immunol* **17:** 467–522

Griffith LC (2004) Receptor clustering: nothing succeeds like success. *Curr Biol* **14:** R413–R415

Homma M, Shiomi D, Homma M, Kawagishi I (2004) Attractant binding alters arrangement of chemoreceptor dimers within its cluster at a cell pole. *Proc Natl Acad Sci USA* **101:** 3462–3467

Kentner D, Sourjik V (2006) Spatial organization of the bacterial chemotaxis system. *Curr Opin Microbiol* **9:** 619–624

Kentner D, Thiem S, Hildenbeutel M, Sourjik V (2006) Determinants of chemoreceptor cluster formation in *Escherichia coli*. *Mol Microbiol* **61:** 407–417

Keymer JE, Endres RG, Skoge M, Meir Y, Wingreen NS (2006) Chemosensing in *Escherichia coli*: two regimes of two-state receptors. *Proc Natl Acad Sci USA* **103:** 1786–1791

Kim KK, Yokota H, Kim SH (1999) Four-helical-bundle structure of the cytoplasmic domain of a serine chemotaxis receptor. *Nature* **400:** 787–792

Lai RZ, Manson JM, Bormans AF, Draheim RR, Nguyen NT, Manson MD (2005) Cooperative signaling among bacterial chemoreceptors. *Biochemistry* **44:** 14298–14307

Lamanna AC, Ordal GW, Kiessling LL (2005) Large increases in attractant concentration disrupt the polar localization of bacterial chemoreceptors. *Mol Microbiol* **57:** 774–785

Li G, Weis RM (2000) Covalent modification regulates ligand binding to receptor complexes in the chemosensory system of *Escherichia coli*. *Cell* **100:** 357–365

Liberman L, Berg HC, Sourjik V (2004) Effect of chemoreceptor modification on assembly and activity of the receptor-kinase complex in *Escherichia coli*. *J Bacteriol* **186:** 6643–6646

Lybarger SR, Maddock JR (1999) Clustering of the chemoreceptor complex in *Escherichia coli* is independent of the methyltransferase CheR and the methylesterase CheB. *J Bacteriol* **181:** 5527–5529

Lybarger SR, Nair U, Lilly AA, Hazelbauer GL, Maddock JR (2005) Clustering requires modified methyl-accepting sites in low-abundance but not high-abundance chemoreceptors of *Escherichia coli*. *Mol Microbiol* **56:** 1078–1086

Maddock JR, Shapiro L (1993) Polar location of the chemoreceptor complex in the *Escherichia coli* cell. *Science* **259:** 1717–1723

McAndrew RS, Ellis EA, Lai RZ, Manson MD, Holzenburg A (2005) Identification of Tsr and Tar chemoreceptor arrays in *E. coli* inner membranes. *Microsc Microanal* **11:** 1190–1191

McAndrew RS, Ellis EA, Lai RZ, Manson MD, Holzenburg A (2006) Effects of chemoreceptor modification on the structures of Tsr arrays. *Microsc Microanal* **12:** 378–379

McAndrew RS, Ellis EA, Manson MD, Holzenburg A (2004) TEM analysis of chemoreceptor arrays in native membranes of *E. coli*. *Microsc Microanal* **10:** 416

Mello BA, Tu Y (2005) An allosteric model for heterogeneous receptor complexes: understanding bacterial chemotaxis responses to multiple stimuli. *Proc Natl Acad Sci USA* **102:** 17354–17359

Mello BA, Tu Y (2007) Effects of adaptation in maintaining high sensitivity over a wide range of backgrounds for *Escherichia coli* chemotaxis. *Biophys J* **92:** 2329–2337

Monod J, Wyman J, Changeux JP (1965) On the nature of allosteric transitions: a plausible model. *J Mol Biol* **12:** 88–118

Press WH, Teukolsky SA, Vetterling WT, Flannery BP (2002) Chapter 11. In *Numerical Recipes in C++: the Art of Scientific Computing*. Cambridge, MA, USA: Cambridge University Press

Schamel WW, Reth M (2000) Monomeric and oligomeric complexes of the B cell antigen receptor. *Immunity* **13:** 5–14

Schulmeister S, Ruttorf M, Thiem S, Kentner D, Lebiedz D, Sourjik V (2008) Protein exchange dynamics at chemoreceptor clusters in *Escherichia coli*. *Proc Natl Acad Sci USA* **105:** 6403–6408

Shiomi D, Banno S, Homma M, Kawagishi I (2005) Stabilization of polar localization of a chemoreceptor via its covalent modifications and its communication with a different chemoreceptor. *J Bacteriol* **187:** 7647–7654

Shrout AL, Montefusco DJ, Weis RM (2003) Template-directed assembly of receptor signaling complexes. *Biochemistry* **42:** 13379–13385

Skoge ML, Endres RG, Wingreen NS (2006) Receptor–receptor coupling in bacterial chemotaxis: evidence for strongly coupled clusters. *Biophys J* **90:** 4317–4326

Sourjik V, Berg HC (2000) Localization of components of the chemotaxis machinery of *Escherichia coli* using fluorescent protein fusions. *Mol Microbiol* **37:** 740–751

Sourjik V, Berg HC (2002) Receptor sensitivity in bacterial chemotaxis. *Proc Natl Acad Sci USA* **99:** 123–127

Sourjik V, Berg HC (2004) Functional interactions between receptors in bacterial chemotaxis. *Nature* **428:** 437–441

Sourjik V, Vaknin A, Shimizu TS, Berg HC (2007) *In vivo* measurement by FRET of pathway activity in bacterial chemotaxis. *Methods Enzymol* **423:** 363–391

Studdert CA, Parkinson JS (2004) Crosslinking snapshots of bacterial chemoreceptor squads. *Proc Natl Acad Sci USA* **101:** 2117–2122

Studdert CA, Parkinson JS (2005) Insights into the organization and dynamics of bacterial chemoreceptor clusters through *in vivo* crosslinking studies. *Proc Natl Acad Sci USA* **102:** 15623–15628

Ursell T, Huang KC, Peterson E, Phillips R (2007) Cooperative gating and spatial organization of membrane proteins through elastic interactions. *PLoS Comput Biol* **3:** e81

Vaknin A, Berg HC (2006) Osmotic stress mechanically perturbs chemoreceptors in *Escherichia coli*. *Proc Natl Acad Sci USA* **103:** 592–596

Weis RM, Hirai T, Chalah A, Kessel M, Peters PJ, Subramaniam S (2003) Electron microscopic analysis of membrane assemblies formed by the bacterial chemotaxis receptor Tsr. *J Bacteriol* **185:** 3636–3643

Yin CC, Blayney LM, Lai FA (2005) Physical coupling between ryanodine receptor–calcium release channels. *J Mol Biol* **349:** 538–546

Zhang P, Khursigara CM, Hartnell LM, Subramaniam S (2007) Direct visualization of *Escherichia coli* chemotaxis receptor arrays using cryo-electron microscopy. *Proc Natl Acad Sci USA* **104:** 3777–3781